ACS APPLIED MATERIALS & INTERFACES

Research Article

www.acsami.org

Novel Hybrid Carbon Nanofiber/Highly Branched Graphene Nanosheet for Anode Materials in Lithium-Ion Batteries

Haejune Kim,[†] Xingkang Huang,[†] Xiaoru Guo, Zhenhai Wen, Shumao Cui, and Junhong Chen*

Department of Mechanical Engineering, University of Wisconsin-Milwaukee, 3200 North Cramer Street, Milwaukee, Wisconsin 53211, United States

Supporting Information

ABSTRACT: The novel hybrid carbon nanofiber (CNF)/highly branched graphene nanosheet (HBGN) is synthesized via a simple two-step CVD method and its application as the anode material in a lithium-ion battery (LIB) is demonstrated. The CNFs offer a good electrical conductivity and a robust supporting structure, while the HBGNs provide increased Li storage sites including nanoporous cavities, large surface area, and edges of exposed graphene platelets. The hybrid material showed a reversible capacity of 300 mAh g^{-1} with excellent cycling stability. Our study provides a new avenue for design and synthesis of carbon−carbon hybrid materials for versatile applications.

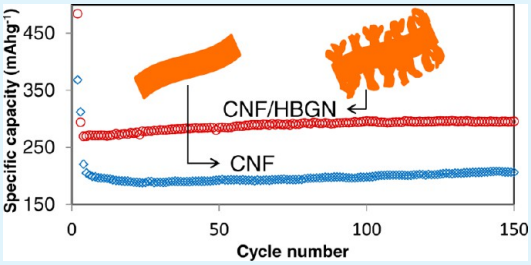

KEYWORDS: *carbon nanofiber, highly branched graphene nanosheet, carbon−carbon hybrid, Li-ion battery, plasma-enhanced chemical vapor deposition, graphene*

INTRODUCTION

Nanostructured carbon exists in various types of allotropes: 0-dimensional fullerenes (C60), 1-dimensional carbon nanotubes (CNTs) and carbon nanofibers (CNFs), and 2-dimensional graphenes (or GNS: graphene nanosheet). Each carbon allotrope that is characterized by its unique shape, dimensionality, and properties can be used as a building block to synthesize new hybrid materials by combining two or more allotropes.[1] Novel hybrids with a new structure and new morphology can be realized by two representative methods: (1) mixing surface-treated carbon materials[2−4] and (2) employing catalytic seeds for 1D carbon growth on 2D graphene.[5−7]

Among these carbon allotropes, the recent discovery of the wonder material graphene has totally changed our view of the nanoscopic world, owing to its special structure and properties.[8−10] Graphene is a one-atom-thick 2D sheet of sp^2-bonded carbon atoms having exceptional mechanical, electrical, and thermal transport properties.[11−13] In particular, graphene exhibits remarkably high electron mobility even at ambient temperatures.[14,15] Graphene can be produced by exfoliating graphite,[16,17] epitaxial growth from a SiC single crystal surface,[18,19] solvothermal reaction,[20] and chemical vapor deposition (CVD).[12,21,22] There have been various approaches to take advantage of the unique properties of graphene in optoelectronics,[23,24] sensing,[25,26] and energy storage.[27−30] Recently, Chae et al. designed a new hybrid of CNT/graphene integrated with a wrinkled Al_2O_3 layer, demonstrating great potential for stretchable and transparent electronics.[31] Kim et al. developed a superelastic and fatigue-resistant 3D-CNT network by coating it with a few layers of graphene, which improves the Young's modulus by a factor of 6.[32] Previously, our group reported a CNT hybrid material covalently bonded with graphene leaves[33] and highly branched graphene nanosheets (HBGNs) directly grown on a planar graphene sheet.[34] HBGNs are a few layered graphene nanosheets with open boundaries, which have similar structural characteristics to carbon nanowalls (CNWs). However, different from CNWs, HBGNs are composed of a highly dense, small graphene domain with less than 5 nm in lateral dimension, and the "standing" graphene sheets are randomly oriented.

In this study, we investigate novel hybrid CNF/HBGN for anode materials for LIB application. HBGNs can be grown on any electrically conductive substrate without adding any catalyst. We used direct growth of CNFs on type 304 stainless steel for hybridizing with HBGNs. In contrast to the loosely bound hybrids prepared by simply mixing two materials or catalytic growth on a graphene surface, the hybrid CNF/HBGN will provide a continuous conduction pathway, which is expected to lead to a high charge carrier mobility. CNFs will offer good electrical conductivity and a robust support structure, while HBGNs offer increased Li storage sites. The controlled synthesis method for hybrid CNF/HBGN will offer insights into the bottom-up design of carbon−carbon bond formation.

The CNF/HBGN synthesis is accomplished through a two-step CVD process. The experimental details can be found elsewhere.[33,35] In brief, the two-step CVD process consists of a CVD method for CNF growth and a plasma-enhanced CVD (PECVD) method for HBGN growth, both of which were catalyst-free atmospheric pressure growth. We modified a CNT

Received: May 27, 2014
Accepted: October 13, 2014
Published: October 13, 2014

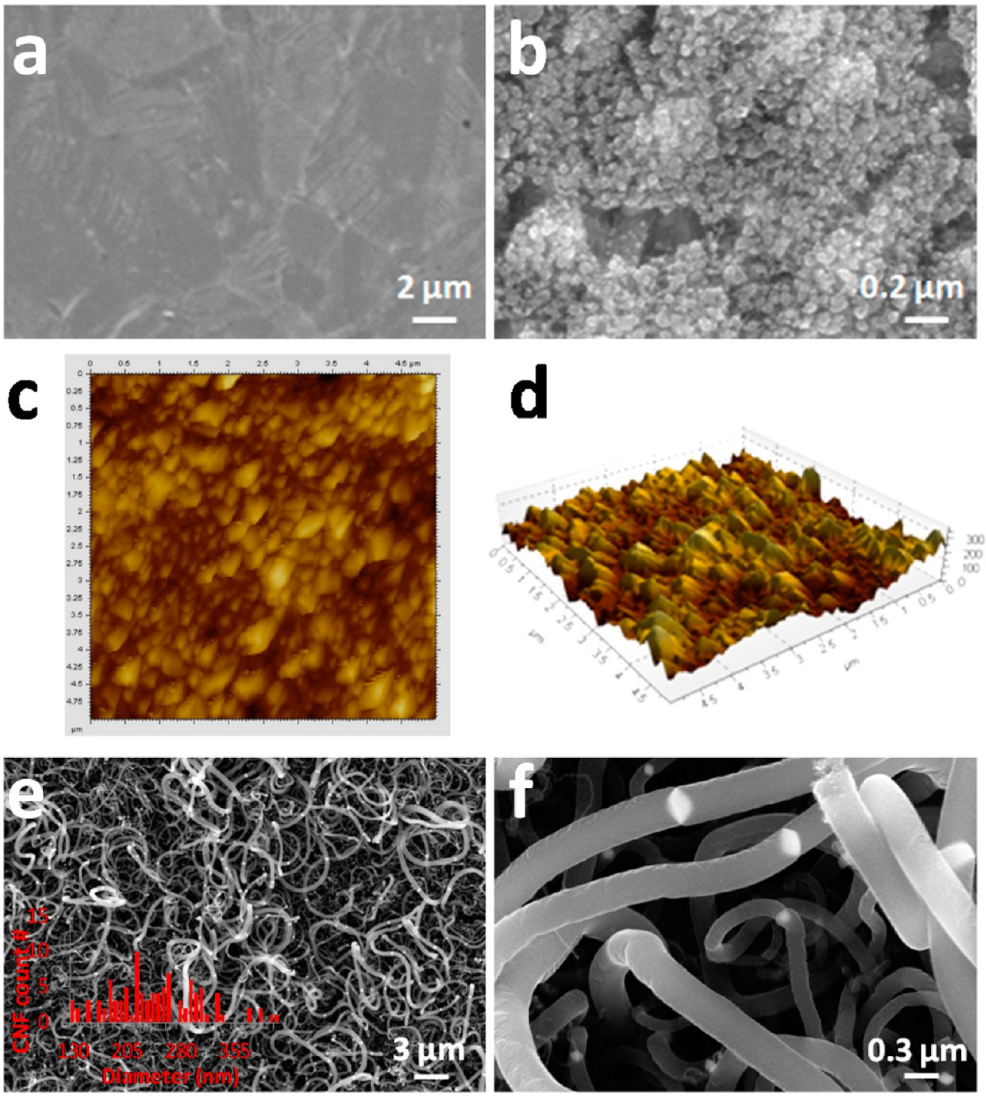

Figure 1. (a) SEM image of as-received stainless steel, (b) SEM image of stainless steel after chemical/thermal treatment, (c, d) AFM topography images of stainless steel after chemical/thermal treatment, and (e, f) SEM images of CNFs grown on stainless steel; inset in Figure 1e shows the histogram of the CNF diameter.

growth method described by Baddour et al.[36] to synthesize CNFs. The CNF growth was conducted without applying additional catalysts that are generally required to nucleate CNFs through C atom diffusion over the catalyst. CNFs were directly grown on type 304 stainless steel (Fe/Cr/Ni = 70:19:11 wt %, Alfa Aesar) that contains a large fraction of iron and nickel. To facilitate the growth of CNFs, the surface condition of stainless steel needs to be modified to create particle-like active catalytic sites. In this pretreatment step, the native passive oxide film (Cr_2O_3) was etched away with 35 wt % hydrochloric acid (HCl) for 10 min. This etching process can be replaced by mechanically polishing the surface of stainless steel without difficulty since the passive oxide layer is only a few nanometers thick. Next, the acid-treated stainless steel was thermally annealed for 30 min at 850 °C in a tube furnace under hydrogen environment. The temperature of the reactor was decreased to 700 °C, and the CNF started to grow under the acetylene, hydrogen and water-containing argon flow. Subsequently, HBGNs were synthesized on the CNF substrate using an atmospheric-pressure direct current (dc) PECVD method as shown in Supporting Information Figure S1. A pin-plate electrode in a quartz tube reactor was equipped with high voltage supply. The two electrodes, separated by about 10 mm, were installed perpendicular to the flow direction, which did not require any conductive paste or fixture to hold the sample. A mixture of acetylene (C_2H_2) and argon (Ar) with water vapor was introduced into the quartz tube in the reactor. The typical flow ratio of C_2H_2 to Ar was 10 and the temperature of the reactor was 700 °C. When a dc voltage of about 3 kV was applied, the dc glow discharge formed between the electrodes and HBGNs started to grow on the surface of CNFs. The dissociated carbon precursors under the glow-discharge plasma nucleated on the surface of CNFs and started to grow perpendicular to the substrate. As the growth continued, more graphene sheets nucleated on the surfaces and edges of pre-existing graphene sheets, producing graphene sheets with a smaller domain size. HBGNs eventually cover the entire surface of the CNFs.

The CNF/HBGN on stainless steel was transferred to the glovebox (H_2O and O_2 level below 1 ppm) for coin cell assembly. The as-produced CNF/HBGN on stainless steel was used as an electrode without binder or conductive additives.

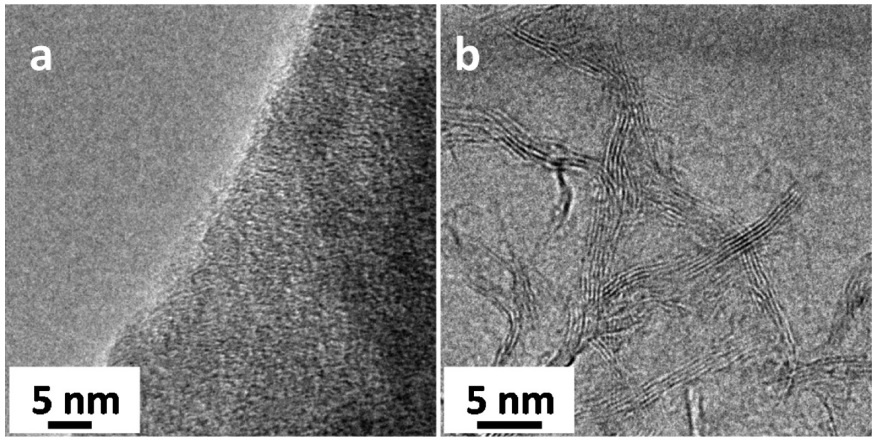

Figure 2. High-resolution TEM images of (a) CNFs and (b) HBGNs.

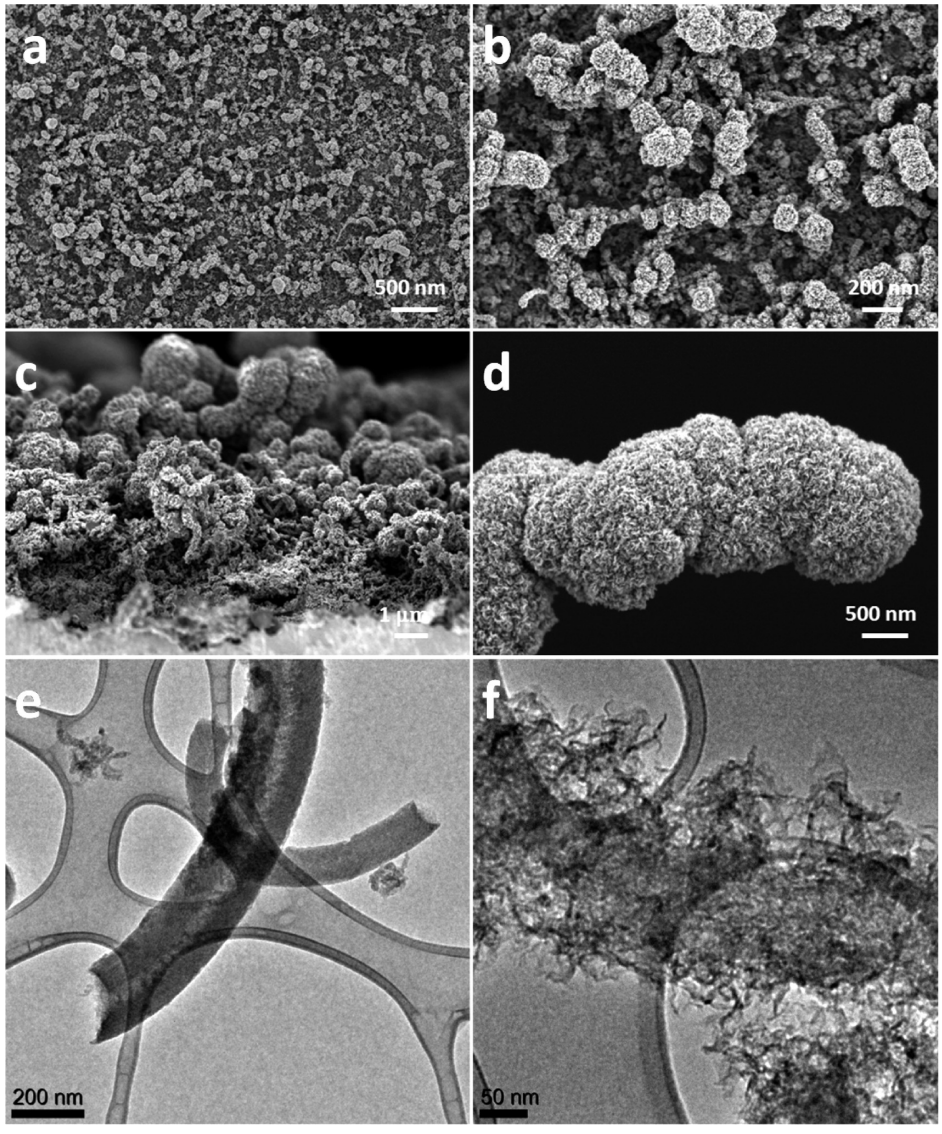

Figure 3. (a, b) SEM images of CNF/HBGN on stainless steel (top view), (c, d) SEM images of CNF/HBGN on stainless steel (side view), (e) TEM image of a bare CNF, and (f) TEM image of a CNF/HBGN hybrid.

The total weight change of CNF/HBGN (loading density: ~0.3 mg cm^{-2}) on stainless steel was measured for capacity calculation before and after the two-step CVD process. A 2032 coin type half-cell was assembled for electrochemical tests with a working electrode, a Celgard 2322 membrane separator, and Li foil as a reference and counter electrode. The electrolyte

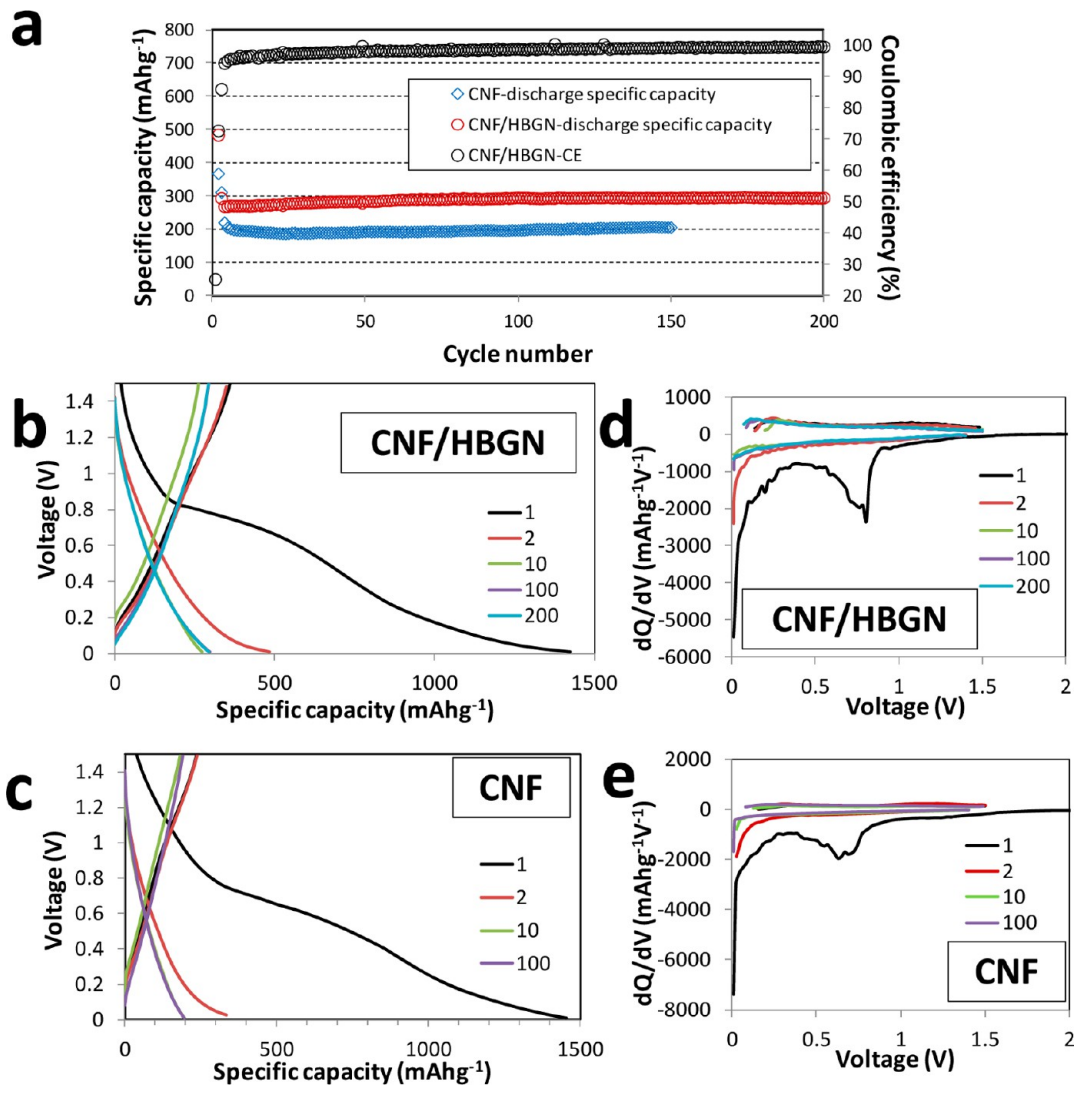

Figure 4. (a) Cycle performance (charge, discharge, and Coulombic efficiency or CE) of CNF/HBGN and CNF electrodes between 0.01 and 1.5 V at a current rate of 0.5 C (or 150 mA g^{-1}) in the first 3 cycles, and 1 C (or 300 mA g^{-1}) for the rest of the cycles, (b) charge/discharge profiles of CNF/HBGN, (c) charge/discharge profiles of CNF, (d) differential capacity (dQ/dV) profiles of CNF/HBGN, and (e) differential capacity (dQ/dV) profiles of CNF.

consisted of 1 M $LiPF_6$ in a nonaqueous solution of ethylene carbonate (EC) and ethyl methyl carbonate (EMC) of 40:60 volume ratio.

The electrochemical charge−discharge cycles were tested at a LAND CT2001A workstation. Electrochemical impedance spectra (EIS) were analyzed using a CHI 660D electrochemical workstation with an amplitude of 10 mV. Scanning electron microscopy (SEM) analysis was performed on a Hitachi S-4800 SEM with a stated resolution of 1.4 nm operated at 1 kV acceleration voltage. Transmission electron microscopy (TEM) analysis was conducted on a Hitachi H 9000 NAR TEM, which has a stated point resolution of 0.18 nm operated at 300 kV in the phase contrast, high-resolution TEM (HRTEM) imaging mode. Brunauer−Emmet−Teller (BET) specific surface area was measured with a Micromeritics ASAP 2020 using the N_2 adsorption at the temperature of liquid nitrogen. Raman measurements were taken using a Reinshaw 100B with a spot diameter of 4 μm and an excitation wavelength of 633 nm.

Type 304 stainless steel contains a high content of iron and nickel, which were used as catalysts to grow CNFs without an additional process to deposit catalysts. In Figure 1a, the SEM image shows the clean surface of as-received stainless steel foil. The stainless steel foil was chemically/thermally treated to facilitate the catalyst island formation on the surface. After chemical/thermal treatment, particle-like catalysts were precipitated on the stainless steel as shown in Figure 1b. The diameter of CNFs is closely associated with the size of the catalyst. The wide diameter distribution of CNFs is attributed to the wide size distribution of precipitated catalyst particles (Figure 1c, d). In Figure 1e, highly dense CNFs grew intertwined with diameters in the range of 100−400 nm (see inset histogram of CNF diameter). Figure 1f shows diamond-shaped catalyst particles located in the middle of the CNF. The CNF continues to grow in two opposite directions on the catalyst face. CNF is an ideal platform for bridging the current collector and active materials, since all CNFs are directly connected to the stainless steel and provide robust mechanical support for the HBGNs.

The morphology of HBGNs is very different from solution-grown graphene, which usually forms a wrinkled paper-like structure. After synthesizing HBGNs on the surface of the CNFs, the diameter of the hybrid was increased. The BET

surface area for the CNFs and HBGNs was found to be 65 and 269 m^2 g^{-1},[34] respectively. The surface area of CNFs was increased by the fusion with HBGNs. In Figure 2, a high resolution TEM image reveals no long-range order in the CNFs, suggesting incomplete graphitization, while the HBGNs shows ordered graphite lattices, indicating the HBGNs are composed of a few layers of graphene. The SEM image in Figure 3a−d clearly shows that the HBGNs totally cover the entire external surface of the CNFs, exposing the edge of the graphene platelet. The diameter of the CNF/HBGN gets thicker at the tip of the CNFs because of the enhanced electric field at the tip. Likewise, denser CNF/HBGNs were observed on the top surface of the electrodes as shown in Figure 3c, which shows a TEM image of the smooth surface of bare CNFs. After ultrasonication of the CNF/HBGNs for 1 h, the hybrid was transferred onto the TEM grid. The surface of the CNF was still covered by graphene sheets, proving that there is strong adhesion between CNF and HBGN, as shown in Figure 3f. The strong adhesion may be attributed to the chemical bonding between a CNF and a HBGN.

Raman spectroscopy was used to investigate the structural properties of the CNF/HBGN hybrid. Supporting Information Figure S2 shows the representative Raman spectra of CNF, HBGN, and CNF/HBGN having characteristic D band and G band. The D band is related to the structural disorder of graphite, and the G band is ascribed to in-plane sp^2 carbon atom vibration, indicating the formation of graphitized structure. The Raman spectrum of the CNFs displays two prominent peaks at 1327 and 1598 cm^{-1}. After the deposition of HBGNs on CNFs, those peaks shifted to 1325 and 1603 cm^{-1}, similar to those seen for HBGNs. Furthermore, the 2D peak at 2659 cm^{-1} and S3 peak at 2905 cm^{-1} appeared, indicating the presence of graphitized structure. However, the intensity ratio of D and G bands (I_D/I_G) for HBGN and CNF/HBGN increased to about 2.2, whereas the I_D/I_G for CNFs is about 1.4. The increase in I_D/I_G suggests that the degree of disorder in the hybrid increased by combining the CNFs with the HBGNs. On the other hand, owing to the unique structure of the HBGNs, the presence of graphene edges that are perpendicular to the substrate can be seen as defects, which may contribute to the increased intensity of the D peak to some degree.[37] When the laser beam is on the graphene edge or when the incident light polarization and the edge are parallel, the D peak intensity becomes strong.

XPS analysis was conducted in order to investigate the surface condition of the acid treated stainless steel. The passive film of chromium oxide on the surface of stainless steel was removed after etching in 35 wt % HCl as shown in Supporting Information Figure S3. XPS results also indicate the iron oxide (Fe $2p_{3/2}$ peak at 711 eV for Fe^{3+}) decreased significantly after acid etching due to the removal of the iron oxide passive film, which was dominant on the top surface of the stainless steel.[38] We also confirm that there was no CNF growth on nontreated stainless steel as opposed to the very dense black CNF growth on the acid treated surface in Supporting Information Figure S4. The patterned growth of CNF/HBGNs is possible by selectively treating the stainless steel substrate in an acid solution.

The CNF/HBGN hybrid was investigated as an anode material for use in LIBs. The electrochemical performance of the CNF/HBGN electrode was tested through a galvanostatic charge (delithiation)/discharge (lithiation) cycle. In Figure 4a, the cycling performance results showed slight improvement in energy density on the CNF/HBGN electrode compared to CNF alone. The increase in energy density of the hybrid materials may be attributed to the increased number of Li storage sites such as the enlarged surface area, edges of graphene films, and nanoporous cavities of the hybrid materials. The reversible capacity of the CNF/HBGNs after 200 cycles stayed at about 300 mAh g^{-1}, while the reversible capacity of CNF alone after 150 cycles was about 200 mAh g^{-1}. Parts b and c of Figure 4 show the charge/discharge profiles of the CNF/HBGN and the CNF electrode, respectively.

The Li intercalation behavior of these electrodes was very similar to each other, but different from that of a conventional graphite electrode. The capacity above 0.5 V is attributed to the faradic capacitance on the surface and edges of the graphene, and the capacity below 0.5 V is due to the Li intercalation into the graphene layers.[39] The discharge voltage profiles did not show a distinct plateau below 0.5 V, which is different from the Li-intercalation into graphite exhibiting a plateau at about 0.1 V.[40] These results indicate that the electrodes may be composed of disorderly stacked graphene sheets.[27] The electrodes exhibited very low Coulombic efficiency (CE), about 25% in the first cycle due to the SEI layer formation on a large surface area, and an irreversible reaction with amorphous carbon impurities and the oxygen-containing functional groups. The electrochemical reactivity was examined by the dQ/dV profiles, which were acquired by numerical differentiation of the galvanostatic cycling data. The SEI formation is clearly evidenced by large peaks at around 0.8 V in Figure 4d and e, which disappeared in the subsequent cycles. It should be noted that there was no measurable weight change on the CNF substrate after $^1/_2$ h of HBGN growth, indicating that the amount of HBGNs was less than 0.005 mg. Uncertainty in the specific capacity calculation according to the precision of the balance (Sartorius CPA225D with a resolution of 0.01 mg) was estimated to be less than 6 mAh g^{-1}.

By coating the CNFs with graphene films, the increased surface area of the hybrid provided more Li-ion storage sites, while CNF provides a strong mechanical support and a good electrical conductivity. Supporting Information Figure S5a shows the Nyquist plot of the CNF anode, tested using a three-electrode cell, exhibiting two semicircles and an inclined line. The first semicircle at high frequencies is related to the SEI layer while the second semicircle at intermediate frequencies is ascribed to the charge transfer process; the inclined line at the low frequency zone is associated with the Li ion diffusion.[41] The impedance spectra were fitted by a Zview software using the equivalent circuit shown in Supporting Information Figure S6. The Ohmic (including the electrolyte resistance and the contact resistance), SEI layer, and charge transfer resistances for the CNF anode were measured as 2.2, 453.9, 168.3, and 342.2 Ohm, respectively. The small Ohmic resistance suggests the good contact between the CNFs and the current collector (stainless steel foil), and the good electrical conductivity of the CNF anode. On the other hand, the SEI layer, charge transfer, and Li ion diffusion resistances for the CNF anode are high, which is consistent with its electrochemical performance, namely, delivering only 200 mAh g^{-1} at 300 mA g^{-1}. In contrast, the Ohmic, SEI layer, charge transfer, and Li ion diffusion resistances for the hybrid CNF/HBGN were 0.88, 14.4, 11.7, and 32.2 Ohm, respectively. This means that all of the resistances were reduced after the growth of HBGNs on the CNFs. The increased specific surface area by HBGNs helped to decrease the resistance, and the thin wall thickness of HBCNs

contributed to the fast charge transfer and Li ion diffusion. As a result, the CNF/HBGN anode exhibited significantly improved performance, namely, delivering 300 mAh g^{-1} at 300 mA g^{-1} (improved by 50% compared with that of the CNF anode). Therefore, the hybridization of the CNFs and HBGNs showed synergistic effects for Li-ion battery applications.

CONCLUSION

In summary, we have developed a simple two-step CVD method to synthesize hybrid CNF/HBGNs for LIB application. The lithium insertion behavior of the CNF/HBGN was studied. Using CNF/HBGNs as anode materials leads to a higher Li storage capability compared to CNF alone. The HBGNs with nanoporous cavities, large surface area, and edges of exposed graphene platelets provide not only more sites for Li-ions to be stored but also high electrical conductivity and chemical stability. Moreover, the covalently bonded hybrid structure and substrate-bound CNFs provide fast ion/electron transfer. The hybrid material shows a reversible capacity of 300 mAh g^{-1} with excellent cycling stability. Higher purity and higher degree of graphitization of as-produced CNFs may be achieved by further chemical and thermal treatment, improving the charge capacity of CNFs, thus overall charge capacity of the hybrid is also expected to increase. With its large surface area and good electrical conductivity, this unique hybrid structure is also promising for supercapacitor applications. Our synthesis methods using PECVD provide a new technique for the design and synthesis of hybrid materials for versatile applications. In addition, commercially available, low cost CNFs will make the fabrication process readily scalable.

ASSOCIATED CONTENT

Supporting Information

Schematic of the experimental setup, Raman spectra of the hybrid, XPS analysis of the acid-treated stainless steel, photo image of CNF coverage on acid-treated and untreated stainless steel, and EIS analysis. This material is available free of charge via the Internet at http://pubs.acs.org.

AUTHOR INFORMATION

Corresponding Author

*Fax: +1-414-229-6958. Tel: +1-414-229-2615. E-mail: jhchen@uwm.edu.

Author Contributions

†H.K. and X.H. contributed equally. The manuscript was written through contributions of all authors. All authors have given approval to the final version of the manuscript.

Notes

The authors declare no competing financial interest.

ACKNOWLEDGMENTS

The authors acknowledge financial support from the Research Growth Initiative Program of the University of Wisconsin–Milwaukee (UWM). The SEM imaging was conducted at the UWM Bioscience Electron Microscope Facility, and TEM analyses were conducted at the UWM Physics HRTEM Laboratory.

REFERENCES

(1) Vajtai, R. *Springer Handbook of Nanomaterials*; Springer: New York, 2013.

(2) Fan, Z.; Yan, J.; Zhi, L.; Zhang, Q.; Wei, T.; Feng, J.; Zhang, M.; Qian, W.; Wei, F. A Three-Dimensional Carbon Nanotube/Graphene Sandwich and Its Application as Electrode in Supercapacitors. *Adv. Mater.* **2010**, *22* (33), 3723–3728.

(3) Tung, V. C.; Chen, L.-M.; Allen, M. J.; Wassei, J. K.; Nelson, K.; Kaner, R. B.; Yang, Y. Low-Temperature Solution Processing of Graphene– Carbon Nanotube Hybrid Materials for High-Performance Transparent Conductors. *Nano Lett.* **2009**, *9* (5), 1949–1955.

(4) Yu, D.; Dai, L. Self-Assembled Graphene/Carbon Nanotube Hybrid Films for Supercapacitors. *J. Phys. Chem. Lett.* **2009**, *1* (2), 467–470.

(5) Lee, D. H.; Kim, J. E.; Han, T. H.; Hwang, J. W.; Jeon, S.; Choi, S. Y.; Hong, S. H.; Lee, W. J.; Ruoff, R. S.; Kim, S. O. Versatile Carbon Hybrid Films Composed of Vertical Carbon Nanotubes Grown on Mechanically Compliant Graphene Films. *Adv. Mater.* **2010**, *22* (11), 1247–1252.

(6) Li, S.; Luo, Y.; Lv, W.; Yu, W.; Wu, S.; Hou, P.; Yang, Q.; Meng, Q.; Liu, C.; Cheng, H. M. Vertically Aligned Carbon Nanotubes Grown on Graphene Paper as Electrodes in Lithium-Ion Batteries and Dye-Sensitized Solar Cells. *Adv. Energy Mater.* **2011**, *1* (4), 486–490.

(7) Seo, D. H.; Yick, S.; Han, Z. J.; Fang, J. H.; Ostrikov, K. K. Synergistic Fusion of Vertical Graphene Nanosheets and Carbon Nanotubes for High-Performance Supercapacitor Electrodes. *ChemSusChem* **2014**, *7*, 2317–2324.

(8) Novoselov, K. S.; Fal, V.; Colombo, L.; Gellert, P.; Schwab, M.; Kim, K. A Roadmap for Graphene. *Nature* **2012**, *490* (7419), 192–200.

(9) Geim, A. K.; Novoselov, K. S. The Rise of Graphene. *Nat. Mater.* **2007**, *6* (3), 183–191.

(10) Ostrikov, K.; Neyts, E.; Meyyappan, M. Plasma Nanoscience: From Nano-Solids in Plasmas to Nano-Plasmas in Solids. *Adv. Phys.* **2013**, *62* (2), 113–224.

(11) Novoselov, K.; Geim, A. K.; Morozov, S.; Jiang, D.; Katsnelson, M.; Grigorieva, I.; Dubonos, S.; Firsov, A. Two-Dimensional Gas of Massless Dirac Fermions in Graphene. *Nature* **2005**, *438* (7065), 197–200.

(12) Li, X.; Cai, W.; An, J.; Kim, S.; Nah, J.; Yang, D.; Piner, R.; Velamakanni, A.; Jung, I.; Tutuc, E. Large-Area Synthesis of High-Quality and Uniform Graphene Films on Copper Foils. *Science* **2009**, *324* (5932), 1312–1314.

(13) Neto, A. C.; Guinea, F.; Peres, N.; Novoselov, K. S.; Geim, A. K. The Electronic Properties of Graphene. *Rev. Mod. Phys.* **2009**, *81* (1), 109.

(14) Du, X.; Skachko, I.; Barker, A.; Andrei, E. Y. Approaching Ballistic Transport in Suspended Graphene. *Nat. Nanotechnol.* **2008**, *3* (8), 491–495.

(15) Areshkin, D. A.; Gunlycke, D.; White, C. T. Ballistic Transport in Graphene Nanostrips in the Presence of Disorder: Importance of Edge Effects. *Nano Lett.* **2007**, *7* (1), 204–210.

(16) Dean, C.; Young, A.; Meric, I.; Lee, C.; Wang, L.; Sorgenfrei, S.; Watanabe, K.; Taniguchi, T.; Kim, P.; Shepard, K. Boron Nitride Substrates for High-Quality Graphene Electronics. *Nat. Nanotechnol.* **2010**, *5* (10), 722–726.

(17) Lee, J. H.; Shin, D. W.; Makotchenko, V. G.; Nazarov, A. S.; Fedorov, V. E.; Kim, Y. H.; Choi, J. Y.; Kim, J. M.; Yoo, J. B. One-Step Exfoliation Synthesis of Easily Soluble Graphite and Transparent Conducting Graphene Sheets. *Adv. Mater.* **2009**, *21* (43), 4383–4387.

(18) Berger, C.; Song, Z.; Li, X.; Wu, X.; Brown, N.; Naud, C.; Mayou, D.; Li, T.; Hass, J.; Marchenkov, A. N. Electronic Confinement and Coherence in Patterned Epitaxial Graphene. *Science* **2006**, *312* (5777), 1191–1196.

(19) Emtsev, K. V.; Bostwick, A.; Horn, K.; Jobst, J.; Kellogg, G. L.; Ley, L.; McChesney, J. L.; Ohta, T.; Reshanov, S. A.; Röhrl, J. Towards Wafer-Size Graphene Layers by Atmospheric Pressure Graphitization of Silicon Carbide. *Nat. Mater.* **2009**, *8* (3), 203–207.

(20) Kuang, Q.; Xie, S.-Y.; Jiang, Z.-Y.; Zhang, X.-H.; Xie, Z.-X.; Huang, R.-B.; Zheng, L.-S. Low Temperature Solvothermal Synthesis of Crumpled Carbon Nanosheets. *Carbon* **2004**, *42* (8), 1737–1741.

(21) Gomez De Arco, L.; Zhang, Y.; Schlenker, C. W.; Ryu, K.; Thompson, M. E.; Zhou, C. Continuous, Highly Flexible, and Transparent Graphene Films by Chemical Vapor Deposition for Organic Photovoltaics. *ACS Nano* **2010**, *4* (5), 2865−2873.
(22) Bae, S.; Kim, H.; Lee, Y.; Xu, X.; Park, J.-S.; Zheng, Y.; Balakrishnan, J.; Lei, T.; Kim, H. R.; Song, Y. I. Roll-to-Roll Production of 30-Inch Graphene Films for Transparent Electrodes. *Nat. Nanotechnol.* **2010**, *5* (8), 574−578.
(23) Eda, G.; Fanchini, G.; Chhowalla, M. Large-Area Ultrathin Films of Reduced Graphene Oxide as a Transparent and Flexible Electronic Material. *Nat. Nanotechnol.* **2008**, *3* (5), 270−274.
(24) Bonaccorso, F.; Sun, Z.; Hasan, T.; Ferrari, A. Graphene Photonics and Optoelectronics. *Nat. Photonics* **2010**, *4* (9), 611−622.
(25) Dua, V.; Surwade, S. P.; Ammu, S.; Agnihotra, S. R.; Jain, S.; Roberts, K. E.; Park, S.; Ruoff, R. S.; Manohar, S. K. All-Organic Vapor Sensor Using Inkjet-Printed Reduced Graphene Oxide. *Angew. Chem., Int. Ed.* **2010**, *49* (12), 2154−2157.
(26) Mao, S.; Cui, S.; Lu, G.; Yu, K.; Wen, Z.; Chen, J. Tuning Gas-Sensing Properties of Reduced Graphene Oxide Using Tin Oxide Nanocrystals. *J. Mater. Chem.* **2012**, *22* (22), 11009−11013.
(27) Yoo, E.; Kim, J.; Hosono, E.; Zhou, H.-s.; Kudo, T.; Honma, I. Large Reversible Li Storage of Graphene Nanosheet Families for Use in Rechargeable Lithium Ion Batteries. *Nano Lett.* **2008**, *8* (8), 2277−2282.
(28) Pumera, M. Graphene-Based Nanomaterials for Energy Storage. *Energy Environ. Sci.* **2011**, *4* (3), 668−674.
(29) Wen, Z.; Wang, X.; Mao, S.; Bo, Z.; Kim, H.; Cui, S.; Lu, G.; Feng, X.; Chen, J. Crumpled Nitrogen-Doped Graphene Nanosheets with Ultrahigh Pore Volume for High-Performance Supercapacitor. *Adv. Mater.* **2012**, *24* (41), 5610−5616.
(30) Mao, S.; Wen, Z.; Kim, H.; Lu, G.; Hurley, P.; Chen, J. A General Approach to One-Pot Fabrication of Crumpled Graphene-Based Nanohybrids for Energy Applications. *ACS Nano* **2012**, *6* (8), 7505−7513.
(31) Chae, S. H.; Yu, W. J.; Bae, J. J.; Duong, D. L.; Perello, D.; Jeong, H. Y.; Ta, Q. H.; Ly, T. H.; Vu, Q. A.; Yun, M. Transferred Wrinkled Al_2O_3 for Highly Stretchable and Transparent Graphene−Carbon Nanotube Transistors. *Nat. Mater.* **2013**, *12* (5), 403−409.
(32) Kim, K. H.; Oh, Y.; Islam, M. Graphene Coating Makes Carbon Nanotube Aerogels Superelastic and Resistant to Fatigue. *Nat. Nanotechnol.* **2012**, *7* (9), 562−566.
(33) Yu, K.; Lu, G.; Bo, Z.; Mao, S.; Chen, J. Carbon Nanotube with Chemically Bonded Graphene Leaves for Electronic and Optoelectronic Applications. *J. Phys. Chem. Lett.* **2011**, *2* (13), 1556−1562.
(34) Kim, H.; Wen, Z.; Yu, K.; Mao, O.; Chen, J. Straightforward Fabrication of a Highly Branched Graphene Nanosheet Array for a Li-Ion Battery Anode. *J. Mater. Chem.* **2012**, *22* (31), 15514−15518.
(35) Yu, K.; Bo, Z.; Lu, G.; Mao, S.; Cui, S.; Zhu, Y.; Chen, X.; Ruoff, R. S.; Chen, J. Growth of Carbon Nanowalls at Atmospheric Pressure for One-Step Gas Sensor Fabrication. *Nanoscale Res. Lett.* **2011**, *6* (1), 1−9.
(36) Baddour, C. E.; Fadlallah, F.; Nasuhoglu, D.; Mitra, R.; Vandsburger, L.; Meunier, J.-L. A Simple Thermal CVD Method for Carbon Nanotube Synthesis on Stainless Steel 304 without the Addition of an External Catalyst. *Carbon* **2009**, *47* (1), 313−318.
(37) Casiraghi, C.; Hartschuh, A.; Qian, H.; Piscanec, S.; Georgi, C.; Fasoli, A.; Novoselov, K.; Basko, D.; Ferrari, A. Raman Spectroscopy of Graphene Edges. *Nano Lett.* **2009**, *9* (4), 1433−1441.
(38) Lorang, G.; Belo, M. D. C.; Simoes, A.; Ferreira, M. Chemical Composition of Passive Films on Aisi 304 Stainless Steel. *J. Electrochem. Soc.* **1994**, *141* (12), 3347−3356.
(39) Yazami, R.; Deschamps, M. High Reversible Capacity Carbon−Lithium Negative Electrode in Polymer Electrolyte. *J. Power Sources* **1995**, *54* (2), 411−415.
(40) Yang, S.; Song, H.; Chen, X. Electrochemical Performance of Expanded Mesocarbon Microbeads as Anode Material for Lithium-Ion Batteries. *Electrochem. Commun.* **2006**, *8* (1), 137−142.
(41) Huang, X. K.; Yang, J.; Mao, S.; Chang, J. B.; Hallac, P. B.; Fell, C. R.; Metz, B.; Jiang, J. W.; Hurley, P. T.; Chen, J. H. Controllable Synthesis of Hollow Si Anode for Long-Cycle-Life Lithium-Ion Batteries. *Adv. Mater.* **2014**, *26* (25), 4326−4332.